刘京广, 赵平, 任维, 等. 模拟自然状况研究针铁矿/水钠锰矿对锑矿区黄壤锑形态的影响[J]. 岩矿测试, 2025, 44(3): 391−405. DOI: 10.15898/j.ykcs.202502280032.
LIU Jingguang, ZHAO Ping, REN Wei, et al. Effects of Goethite/Birnessite on Antimony Speciation in Yellow Soil from an Antimony Mining Area under Simulated Natural Conditions[J]. Rock and Mineral Analysis, 2025, 44(3): 391−405. DOI: 10.15898/j.ykcs.202502280032.

模拟自然状况研究针铁矿/水钠锰矿对锑矿区黄壤锑形态的影响

刘京广[1]，赵平[2*]，任维[2]，马雪[1]，何开颖[1]，朱霞萍[1*]
(1. 成都理工大学材料与化学化工学院 (锂资源与锂电产业学院)，四川 成都 610059；
2. 贵州省地质矿产勘查开发局一〇五地质大队，贵州 贵阳 550018)

摘要： 锑矿区及周边土壤锑污染严重，锑污染程度与其在土壤中的存在形态关系密切。铁锰氧化物是土壤黏土矿物中最活跃的成分，影响着锑在土壤中的形态转化。现有研究更多关注铁锰氧化物单一矿物对外源锑吸附的影响，而铁锰氧化物对实际土壤中锑形态转化的影响方面的基础研究有待加强。本文将土壤中常见的针铁矿 (α-FeOOH) 和水钠锰矿 (δ-MnO_2) 以原位制备的方式，分别负载在贵州晴隆锑矿区的锑污染黄壤 (原土) 中，制得载铁土和载锰土，模拟土壤自然状况，淹水 180 天，探究了 α-FeOOH 和 δ-MnO_2 介导下土壤锑形态的转化特征。结果表明，淹水改变了土壤氧化还原特性，影响铁锰氧化物的赋存形态，进而影响锑的形态分布，负载的 α-FeOOH 主要以无定形铁存在，负载的 δ-MnO_2 以游离锰、无定形锰和络合锰三种形式存在。与原土相比，载铁土悬浮液锑和弱酸提取态锑含量分别降低 88.3%～94.4%、21.1%～65.9%，可还原态锑和可氧化态锑含量分别增加 49.0%～67.2%、74.3%～159%；载锰土中悬浮液锑、弱酸提取态锑和可还原态锑分别增加 14.2%～59.5%、6.50%～32.6%、4.80%～23.3%，可氧化态锑降低 16.2%～58.5%。即原土、载铁土和载锰土各形态铁、锰、锑在淹水 30 天变化明显或是变化趋势发生转折，负载 α-FeOOH 促进了土壤弱酸提取态锑向土壤可还原态锑和可氧化态锑转化，负载 δ-MnO_2 促进了土壤可氧化态锑向土壤弱酸提取态锑和可还原态锑转化。该研究为锑污染土壤的风险评估和修复技术提供了关键科学依据，对土壤锑污染的控制需结合铁锰氧化物形态调控和氧化还原条件管理，以实现锑的长期稳定化。

关键词： α-FeOOH；δ-MnO_2；土壤；锑；形态转化；原子吸收光谱法

要点：

(1) α-FeOOH 和 δ-MnO_2 是土壤黏土矿物中最活跃的成分，影响着锑在土壤中的形态转化。以原位制备的方式负载 4.0% α-FeOOH(以铁计) 和 0.1% 的 δ-MnO_2(以锰计)，获得载铁土和载锰土。

(2) 负载的 α-FeOOH 在土壤中主要以无定形铁为主；负载的 δ-MnO_2 在土壤中以多种形态锰存在。

(3) 原土/载铁土/载锰土各形态铁、锰、锑在淹水 30 天变化明显或变化趋势发生转折，淹水使土壤中铁锰氧化物形态发生变化，进一步促进了锑形态的转化。

中图分类号： X53 **文献标识码：** A

世界卫生组织 (WHO) 建议的土壤锑 (Sb) 最大允许浓度为 36mg/kg[1]，然而在全球各大锑矿区及其周边土壤都存在严重的锑污染。在苏格兰格兰丁尼的路易莎矿的矿石加工区和矸石堆有关的土壤中

收稿日期： 2025−02−28；**修回日期：** 2025−04−11；**接受日期：** 2025−04−14；**网络出版日期：** 2025−05−15
基金项目： 国家自然科学基金项目 (42267009)；贵州省地矿局科技计划项目 (黔地矿科合 [2023]10 号)
第一作者： 刘京广，硕士，研究方向：重金属污染土壤修复。E-mail：1521162917@qq.com。
通信作者： 赵平，博士，研究员，研究方向：自然资源调查与综合利用。E-mail：408658867@qq.com。
通信作者： 朱霞萍，博士，教授，研究方向：水土污染防控与修复。E-mail：zhuxiaping@cdut.edu.cn。

锑的最大浓度为 1504.2mg/kg[2]。Ning 等[3]研究发现英格兰东北部泰恩河北岸锑冶炼厂附近的土壤中锑含量高达 1489mg/kg,在废弃的 Cu、Pb、Zn、Sb 四个矿区周围的土壤中检测到 Sb 含量也都在 700mg/kg 左右。中国西南地区存在有大面积低温成矿域的湘、黔锑矿带,全国约有 79% 的锑来源于此,该区域著名的含锑矿包括湖南锡矿山、广西大厂锑矿、贵州独山锑矿、晴隆锑矿等,所以西南地区的局部地表环境可能是中国乃至世界上锑污染较为典型的地区[4]。湖南锡矿山锑矿区农田土壤锑含量介于 141.92 ~ 8733.26mg/kg[5]。根据本项目组前期的调查,贵州晴隆锑矿区周围土壤锑污染更为严重,含量最高达 23559mg/kg[6]。土壤中锑通过食物链进入人体,对心血管、呼吸系统和肝脏等都会造成危害,甚至引发癌症[7]。

锑的毒性大小不仅与其总量有关,很大程度上还取决于其存在形态、价态及其结合态[8]。自然状态下土壤中不同形态锑处于一种动态平衡,活性较大的铁锰氧化物及其形态分布是影响土壤锑形态分布和转化的主要因素[9-10]。铁氧化物,是土壤中极为活跃的成分之一,由于其出色的吸附能力和生物反应性,铁氧化物在土壤中扮演着多重重要角色,如有助于钝化和固定重金属,参与有机质的矿化与积累,影响着养分元素的利用等众多环境过程[11]。目前,已经报道的铁氧化物共有 16 种[12],其中针铁矿[13]、赤铁矿[14]、磁铁矿[15]、无定形铁[16](FeOOH)、零价铁 (ZVI)[17] 和水合铁[18]等均能很好地吸附 Sb(Ⅲ) 和 Sb(Ⅴ)。针铁矿 (α-FeOOH) 是土壤中最常见的铁氧化物,具有化学稳定性好、比表面积大以及颗粒结构细微等特点,其表面存在丰富的羟基基团,可提供大量活性位点,对重金属具有较强的化学亲和力[19-20]。针铁矿对 Sb(Ⅲ) 在很宽 pH 范围 (3 ~ 12) 表现出很好的吸附特性,而在 pH＜7 对 Sb(Ⅴ) 有最大吸附量[21]。在还原条件下,针铁矿中的 Fe(Ⅲ) 作为微生物呼吸作用的末端电子受体,可导致水中 Fe(Ⅱ) 的生成,而 Fe(Ⅱ) 的存在有利于针铁矿重结晶,这使吸附在针铁矿表面的 Sb(Ⅴ) 很容易融入其结构中,增强其稳定性[22]。Shangguan 等[23] 通过 X 射线光电子能谱研究发现,土壤吸附 Sb(Ⅴ) 后 Fe2p 和 O1s 结合能下降,可能是电子在 Sb 和 Fe 之间通过氧化还原反应发生了转移。Guo 等[24] 通过 X 射线光电子能谱 (XPS) 和 X 射线精细结构谱 (XAFS) 观察到 Sb(Ⅲ) 无论是被水合铁氧化物吸附还是沉淀,都可能被氧化成 Sb(Ⅴ)。锰氧化物是自然环境中强氧化剂,通过氧化和吸附机理影响锑在土壤中迁移和转化。其中,水钠锰矿 (δ-MnO_2) 是土壤滞留锑的最佳反应矿物相,除了对 Sb(Ⅲ) 和 Sb(Ⅴ) 均具有吸附能力外[25],矿物表面上的 Mn(Ⅳ) 对 Sb(Ⅲ) 还具有较高的氧化能力。Sun 等[26] 认为该氧化反应是质子驱动进行的,在一定 pH 范围内,随着酸度增加,吸附增强,其中与 δ-MnO_2 直接吸附 Sb(Ⅴ) 不同,Sb(Ⅲ) 的氧化破坏了 δ-MnO_2 的表面结构,并暴露出更多的活性位点,因此,δ-MnO_2 对 Sb(Ⅴ) 的吸附强度随着 Sb(Ⅲ) 的氧化而增强。此外,通过 XPS、EXAFS 和 ATR-FTIR 等技术手段,证实了 Sb(Ⅴ) 主要吸附在 δ-MnO_2 的边缘位置,形成了 MnO(H)-Sb(Ⅴ) 的单齿单核配合物[27]。

现有文献多是研究不同类型的铁、锰氧化物的单矿物在较短时间内对锑的吸附、氧化、沉淀作用,但是,自然界的铁锰氧化物是与复杂基体的土壤共存的,且自身存在多种形态。长时间的淹水实验设计,能够捕捉铁锰氧化物动态转化及 Sb 形态变化过程,更符合自然土壤系统中氧化还原反应和生物地球化学循环的动力学特征,弥补了短期实验仅反映瞬时机制的局限性[28-29]。因此,本文模拟土壤自然状况,选取土壤中普遍存在的 α-FeOOH 和 δ-MnO_2 作为铁、锰氧化物代表,以原位制备的方式负载在锑含量为 16795mg/kg 的黄壤 (原土) 中,制得载铁土和载锰土,淹水 180 天,测定悬浮液铁、锰、锑含量及土壤各形态铁、锰、锑含量,探究了 α-FeOOH 和 δ-MnO_2 介导下土壤锑形态的转化,揭示铁锰氧化物对土壤锑形态的影响机制,为锑矿区土壤锑污染的评估、预警和治理提供理论参考。

1　实验部分

1.1　供试土壤样品

本研究使用的土壤样品采自贵州省黔西南布依族苗族自治州晴隆县。采用混合采样法,即每个采样点周围采集 5 ~ 8 个子样点,混合后缩分,保留 1kg 代表性样品封装好。土壤经过自然风干,研磨过 60 目筛备用。土壤主要成分为石英和高岭土,pH 为 4.20,属于强酸性土壤,有机质含量为 10.9g/kg,阳离子交换容量为 13.1cmol/kg,属于中低有机质土壤,肥力较好。土壤锑含量高达 16796mg/kg,远超贵州省土壤背景值 (2.24mg/kg)[30]。

1.2　仪器和主要试剂

AA-7001 原子吸收分光光度计 (北京东西分析仪器有限公司),测定锑/铁/锰的仪器参数分别为:

波长 217.6nm/248.3nm/279.5nm, 灯电流 4mA/3mA/3mA, 狭缝均为 0.2nm。

THZ-82 数显恒温水浴振荡器 (上海程捷仪器设备有限公司); BGZ-240 电热鼓风干燥箱 (上海博讯实业有限公司); KH19A 高速离心机 (湖南凯达科学仪器有限公司); MA-H-Pro 数显加热型圆盘磁力搅拌 (北京大龙兴创实验仪器股份公司); DXY-7L 数显恒温水浴锅 (东莞三量量具有限公司); KH-100DE 数控超声波清洗器 (昆山禾创超声仪器有限公司); PHS-3CpH 计 (上海雷磁仪器有限公司)

土壤原位负载 α-FeOOH 和 δ-MnO_2 所用试剂: 六水合硝酸铁、氢氧化钠、一水合硫酸锰、高锰酸钾。

测定土壤理化性质所用试剂: 重铬酸钾、硫酸、氯化铵、乙醇。

土壤中各形态铁锰测定所用试剂: 柠檬酸钠、草酸铵、焦磷酸钠、硫酸钠。

土壤中各形态锑测定所用试剂: 乙酸、盐酸羟胺、乙酸铵、过氧化氢、硝酸、盐酸、氢氟酸、高氯酸、锑元素标准溶液 (GSB: 04-1748-2004)。

所用试剂均为分析纯 (>99.99%)。

1.3　实验方法

1.3.1　原土原位负载 α-FeOOH 和 δ-MnO_2 制备载铁土和载锰土的实验方法

根据吴琼等[31]所述的 α-FeOOH 制备方法, 在锑污染黄壤上以原位制备的方式负载 4.0% α-FeOOH(以铁计), 得到载铁土。根据梁慧锋等[32]所述的 δ-MnO_2 制备方法, 在锑污染黄壤上以原位制备的方式负载 0.1% 的 δ-MnO_2(以锰计), 得到载锰土。

通过 X 射线衍射分析确认了 α-FeOOH 和 δ-MnO_2 的结构, 负载针铁矿/水钠锰矿后土壤也进行了 X 射线衍射分析 (图 1)。FeOOH-Soil(载铁土) 在 2θ=21.22°、36.65°、41.19°处的特征峰分别对应 FeOOH 的 (110)、(111)、(140) 晶面, 与针铁矿的标准卡片 PDF#29-0713 相一致; δ-MnO_2-Soil(载锰土) 在 2θ=37.52°、56.37°处的特征峰分别对应 δ-MnO_2 的 (211)、(600) 晶面, 与水钠锰矿的标准卡片 PDF#44-0141 相一致。

1.3.2　土壤淹水实验方法

分别称取 20.0g 锑污染黄壤 (原土)、载铁土和载锰土于 100mL 烧杯中, 以水土比 1∶1.5 添加 30mL 超纯水, 淹水 10、20、30、60、90、120、150 和 180 天, 每个时间处理设置 3 个平行。在淹水期间, 每隔数日, 通过称重法补充挥发的水分, 并搅动均匀。实验结束后, 离心, 测定悬浮液中的锑、铁、锰含量; 土壤烘干通过 60 目筛, 测定土壤各形态的锑、铁、锰含量。

1.3.3　土壤各形态铁/锰/锑提取方法

土壤游离铁/锰采用连二钠硫酸钠-柠檬酸钠-重碳酸钠法提取; 无定形铁/锰采用草酸铵缓冲溶液 (pH=3.2) 提取; 络合铁/锰采用碱性焦磷酸钠溶液 (含 10% 硫酸钠, pH=8.5) 提取。

土壤弱酸提取态锑、可还原态锑、可氧化态锑以及残渣态锑的提取方法参照 GB/T 25282—2010 所述方法。弱酸提取态锑用乙酸提取, 可还原态锑用过氧化氢和乙酸铵溶液提取, 可氧化态锑用盐酸羟胺溶液提取, 残留土壤经洗涤、离心、烘干, 称取烘干土壤用盐酸-硝酸-氢氟酸-高氯酸混合酸消解, 得到残渣态锑。

1.4　土壤各形态铁/锰/锑测定方法和测试数据质量控制

淹水过后, 通过离心和过滤将土壤和悬浮液分开, 保证土壤全部被回收。测定土壤总锑和土壤各形态锑, 各形态锑加和与土壤总锑的绝对差值控制

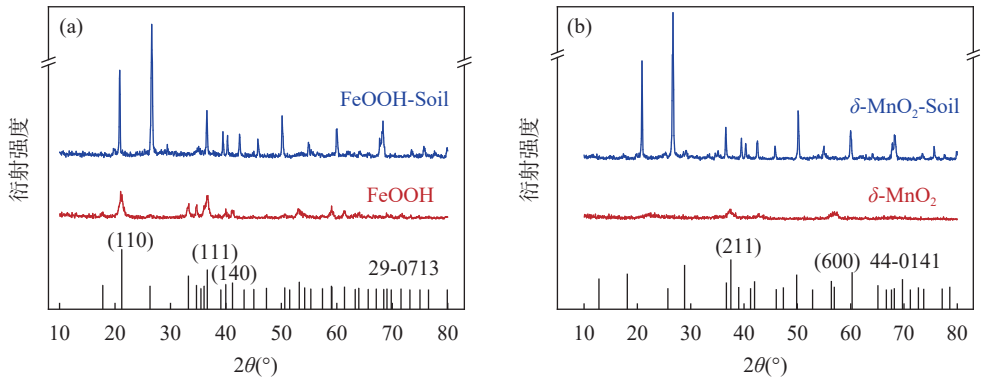

图1　针铁矿/水钠锰矿以及载铁、载锰土壤的 X 射线衍射图谱

Fig. 1　X-ray diffraction patterns of α-FeOOH, δ-MnO_2, Fe-loaded soil and Mn-loaded soil.

在 10% 以内，确保分析质量。悬浮液中的锑、铁、锰含量和土壤各形态锑、铁、锰含量均使用原子吸收光谱法测定，各样品处理均平行三次，结果取平均值，并计算相对标准偏差。以各提取液为试剂空白，火焰原子吸收光谱法测定铁、锰、锑的线性范围为 0.1 ~ 7.0mg/L、0.1 ~ 5.0mg/L、0.2 ~ 20mg/L，决定系数 (R^2) 分别为 0.9991、0.9994、0.9994，相对标准偏差为 2.9%、3.0%、0.77%，检出限分别为 0.0707mg/L、0.0263mg/L、0.0842mg/L。

2　结果与讨论

2.1　淹水时间对原土/载铁土/载锰土铁锰锑释放的影响

根据淹水时间对悬浮液铁锰锑含量的影响结果 (图 2) 可知，原土、载铁土、载锰土悬浮液铁、锰和锑含量随淹水时间变化总趋势基本一致，均随淹水时间的延长而降低。

由图 2a 可知，随淹水时间延长到 180 天，原土悬浮液铁从 589mg/L 降至 125mg/L，下降了 78.8%；载铁土和载锰土悬浮液铁分别从 60.0mg/L 和 137mg/L 降至 4.00mg/L 和 57mg/L，下降了 93.3% 和 58.4%。悬浮液铁含量：原土＞载锰土＞载铁土，原土的悬浮液铁含量最大，淹水前 30 天下降幅度大，直到淹水 150 天变化趋势趋缓，溶出的是原土中可溶性铁。载铁土悬浮液铁含量低于原土 88.8% ~ 97.1%，尽管 α-FeOOH 负载量大，但载铁土悬浮铁含量仍是最低的，因为负载的 α-FeOOH 稳定，不容易被水浸出；载锰土悬浮液铁含量低于原 53.6% ~ 78.9%，因为负载的 δ-MnO_2 对 Fe(Ⅱ) 有一定吸附能力。

由图 2b 可知，随淹水时间延长到 180 天，原土悬浮液锰含量从 12.1mg/L 降至 1.00mg/L，下降了 91.7%；载铁土和载锰土悬浮液锰含量分别从 0.216mg/L、123mg/L 降至 0.0767mg/L、51.0mg/L，下降了 64.5% 和 58.6%。原土的悬浮液锰降低幅度最大，特别在淹水前 30 天，直到淹水 150 天基本稳定，溶出的是原土中可溶性锰。与悬浮液铁变化不同的是：悬浮液锰含量顺序为载锰土＞原土＞载铁土，载锰土悬浮液锰含量高于原土 87.4% ~ 98.2%，负载的锰易溶，但在 180 天的淹水期间，悬浮液锰含量出现反复，是可溶性锰在土壤上发生了吸附解吸。载铁土悬浮液锰含量最低，低于原土 87.5% ~ 98.2%，可能是负载的 α-FeOOH 具有大量的表面活性位点，能够快速吸附可溶性锰。

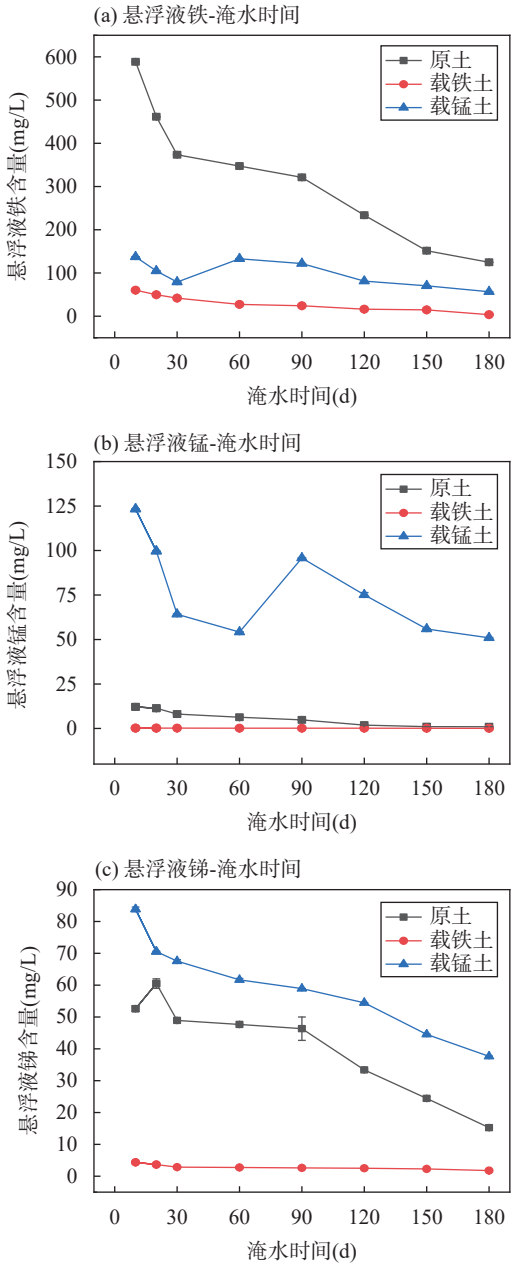

图2　淹水时间对悬浮液铁锰锑含量的影响

Fig. 2　Effect of flooding time on Fe, Mn and Sb content in suspension (a: Suspension iron-flooding time; b: Suspension manganese-flooding time; c: Suspension antimony-flooding time).

由图 2c 可知，随着淹水时间的延长，原土中悬浮液锑含量从 52.6mg/L 降至 15.2mg/L，下降了 71.1%；载锰土和载铁土悬浮液锑含量从 83.9mg/L、4.36mg/L 降至 37.6mg/L、1.78mg/L，下降了 55.1% 和 59.4%。悬浮液锑含量顺序为：载锰土＞原土＞载铁土，与悬浮液锰含量释放顺序一致，载铁土悬浮液锑含量低于原土 88.3% ~ 94.4%，土壤载铁后，

α-FeOOH 可以通过静电吸附、配体交换、表面沉淀和络合作用等吸附水溶性的锑; 载锰土悬浮液锑含量高于原土 14.2% ~ 59.5%, 土壤载锰后, 虽然 δ-MnO_2 也能吸附锑, 但 δ-MnO_2 易溶, 长时间淹水后, 携带吸附的锑进入溶液中。

2.2　淹水时间对原土/载铁土/载锰土中铁和锰形态的影响

2.2.1　淹水时间对原土/载铁土铁形态的影响

图 3 为原土、载铁土各形态铁的含量随淹水时间的变化情况。各形态铁含量变化趋势有差异, 但均在淹水 30 天变化明显或是变化趋势发生转折。

根据图 3a, 原土游离铁含量随淹水时间的延长先降低后增加, 到淹水 90 天时, 降低 12.6%, 之后随淹水时间的延长, 游离铁含量回升, 最终降低 4.00%; 随着淹水时间延长, 载铁土游离铁含量持续降低, 到淹水 180 天时共降低了 10.1%。游离铁是包被于土壤胶体表面的铁氧化物, 是土壤正电荷和负电荷的主要载体, 对重金属离子和含氧酸根离子具有专性吸附功能。

根据图 3b, 原土无定形铁含量随淹水时间的延长增加了 62.7%。载铁土无定形铁含量随淹水时间的延长先增加后下降, 但整体变化不超过 4.50%。无定形铁是游离铁中活性更高的部分, 拥有巨大的比表面积, 对阴阳离子的专性吸附更强。

根据图 3c, 原土和载铁土络合铁含量均随淹水时间的延长而增加, 原土和载铁土中络合铁分别由 1008mg/kg 和 1378mg/kg 增至 1718mg/kg 和 3480mg/kg, 分别增长了 70.4% 和 153%。淹水使铁的反应活性增强, 与土壤中有机质的羟基、羧基、氨基等反应形成络合铁。

与原土相比, 游离铁含量为原土的 2.50 倍, 游离铁包括未被硅酸盐矿物固定的氧化铁, 负载后铁氧化物直接以游离态形式附着于土壤颗粒表面, 或通过快速沉淀形成松散结合的氧化物, 导致游离铁含量显著升高[33]。无定形铁含量为原土的 10.2 倍, 无定形铁是铁氧化物中活性最高的形态, 负载过程中引入的铁因未经历长期成土过程的风化与结晶, 主要以非晶态或弱结晶态存在, 故其含量远超原土[34]。络合铁含量为原土的 2.00 倍, 土壤有机质可通过螯合作用固定 Fe^{3+}, 形成稳定的有机-铁络合物 (如腐植酸铁)。土壤有机质与有机结合态铁呈极显著正相关, 负载后有机质的增加可能进一步促进络合态铁的形成[35]。

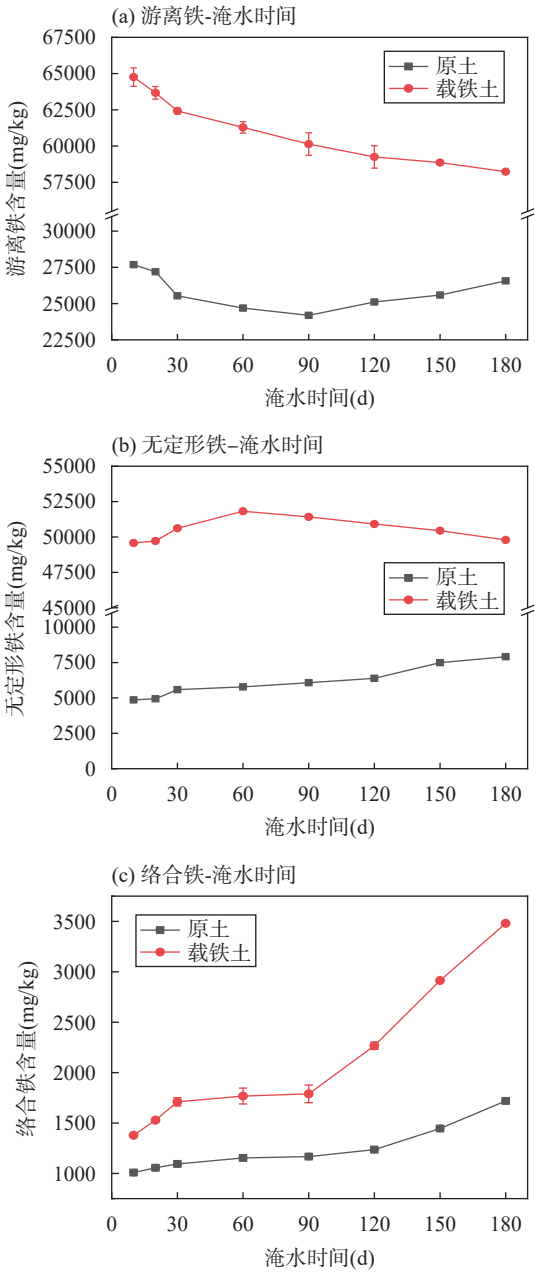

图3　淹水时间对土壤铁形态的影响

Fig. 3　Effect of flooding time on various forms of Fe in soil (a: Free iron-flooding time; b: Amorphous iron-flooding time; c: Complex iron-flooding time).

2.2.2　淹水时间对原土/载锰土锰形态的影响

根据淹水时间对土壤锰形态的影响情况 (图 4), 随淹水时间的延长, 原土各形态锰均随淹水时间延长而增加, 载锰土各形态锰随淹水时间呈现增加-下降-平衡趋势。

根据图 4a, 在 180 天淹水期间, 原土中游离锰含量范围为 21.9 ~ 34.5mg/kg, 增加速率比较均匀, 共增加了 57.5%。以 30 天为节点, 在 10 ~ 30 天中, 载锰

土游离锰含量增加了 25.9%。淹水 30 天后，游离锰含量下降，从 303mg/kg 降至 227mg/kg，降低了 25.1%，到 180 天，下降到初始浓度。

根据图 4b，原土无定形锰含量随淹水时间的延长持续增加，淹水 180 天后，增加了 121%。以 30 天为节点，在 10～30 天中，载锰土中无定形锰增加了 55.1%。淹水 30 天后，无定形锰从 321mg/kg 降至 217mg/kg，降低了 32.2%。总体增加了 5.10%。

根据图 4c，原土络合锰含量随淹水时间的延长而增加，淹水 180 天后，增加了 62.6%。以 30 天为节点，在 10～30 天中，载锰土络合锰增加了 28.5%，淹水 30 天后络合锰从 112mg/kg 降至 77.6mg/kg，降低了 30.7%，到 180 天，下降到初始浓度。

与原土相比，载锰土三种形态锰均远高于原土，游离锰、无定形锰和络合锰含量约为原土的 11.0 倍、25.5 倍和 20.6 倍，说明负载的 δ-MnO_2 以多种形态存在于土壤中。但是三种形态的锰含量在淹水 30 天出现转折，在 90～120 天趋于平稳，接近于淹水初始。载锰土锰形态显著高于原土的成因是 δ-MnO_2 的高反应活性。δ-MnO_2 具有层状结构和丰富的表面羟基，比表面积大（可达 200～300m²/g），易通过吸附、氧化还原或共沉淀作用释放多种形态锰（游离态、无定形态、络合态）。研究表明，δ-MnO_2 在土壤中可发生部分溶解或表面络合反应，显著提升可提取态锰含量，尤其是无定形锰和有机络合锰，证明其多形态赋存特性[36]。

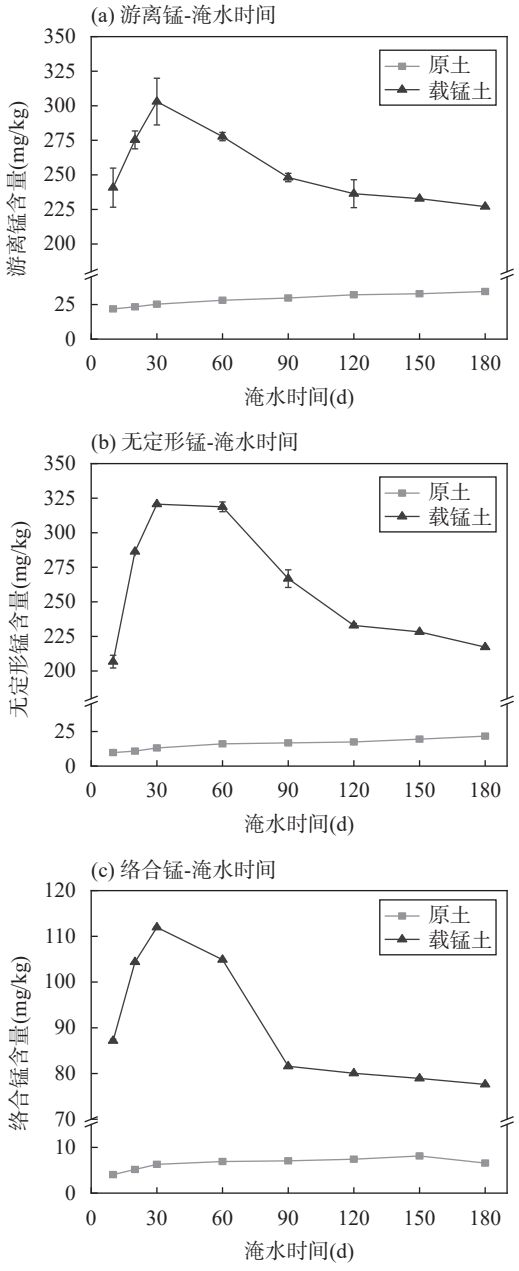

图4　淹水时间对土壤锰形态的影响

Fig. 4　Effect of flooding time on various forms of Mn in soil (a: Free manganese-flooding time; b: Amorphous manganese-flooding time; c: Complex manganese-flooding time).

2.3　淹水时间对原土/载铁土/载锰土锑形态的影响

由图 5a 可知，原土和载锰土弱酸提取态锑含量均随着淹水时间的延长而下降，分别从 123mg/kg 和 140mg/kg 降至 71.9mg/kg 和 107mg/kg，降低了 41.5% 和 23.6%。以 30 天为节点，载铁土弱酸提取态锑含量随淹水时间的延长呈先降低后增加的趋势，整体上弱酸提取态锑含量增加 31.3%。弱酸提取态含量顺序为载锰土＞原土＞载铁土，与原土相比，载铁土弱酸提取态锑含量降低 21.1%～65.9%。与载铁土相反，载锰土弱酸提取态锑含量高于原土 6.50%～32.6%。弱酸提取态锑是被静电吸附在土壤颗粒表面，可被离子交换释放的锑形态以及束缚在碳酸盐中的锑形态，是土壤中活性强的部分，负载的 α-FeOOH 主要以无定形形式存在，对活性锑的吸附能力强，负载的 δ-MnO_2 虽然也能吸附锑，但易于溶解，吸附的锑容易再度释放。

由图 5b 可知，原土、载铁土和载锰土可还原态锑含量随淹水时间的延长均以淹水 30 天为节点，呈先增加后下降的趋势。原土第一个阶段可还原态锑含量增加 16.6%；第二个阶段可还原态锑含量降低了 28.1%，整体上，可还原态锑含量降低 16.2%。载铁土第一和第二阶段可还原态锑含量分别增加了 15.7% 和降低了 21.9%。载锰土可还原态锑含量第一阶段和第二阶段分别增加 14.7% 和降低 16.8%，整体仅变化了 1.80%。可还原态锑含量顺序为载铁土

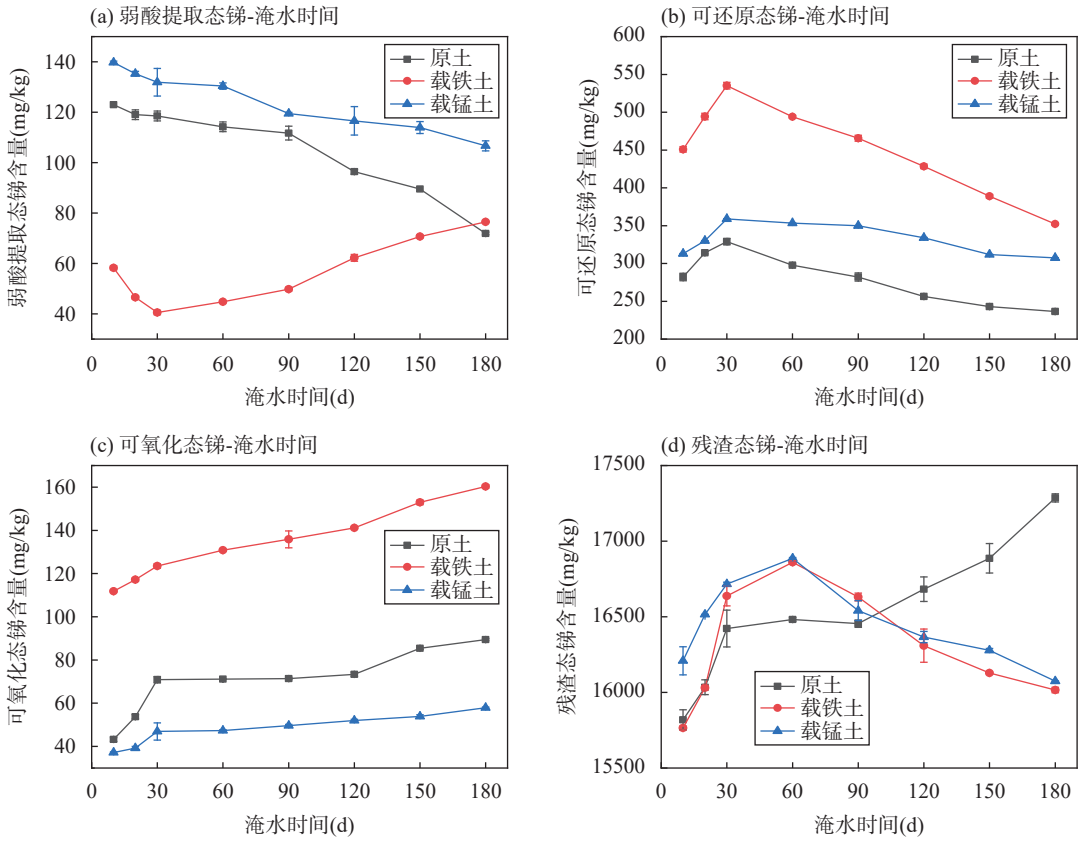

图5　原土/载铁土/载锰土锑形态变化的对比

Fig. 5　Comparison of Sb speciation changes in original soil/Fe-loaded soil/Mn-loaded soil (a: Weak acid extracted antimony-flooding time; b: reducible antimony-flooding time; c: oxidizable antimony-flooding time; d: residual antimony-flooding time).

>载锰土>原土, 与原土相比, 载铁土和载锰土中可还原态锑含量分别高于原土的 49.0% ~ 67.2% 和 4.80% ~ 23.3%。可还原态锑是被氧化铁、氧化锰等吸持的土壤锑形态。载铁和载锰之后, 土壤各形态铁锰显著增加, 因此吸附了大量的锑。而负载的铁主要以无定形形式存在, 锰以三种形式同时存在, 无定形铁活性最强, 拥有巨大的比表面积, 对锑的专性吸附更强, 因而载铁土可还原态锑含量远高于载锰土和原土。

由图 5c 可知, 原土、载铁土和载锰土可氧化态锑含量随着淹水时间的延长均逐渐增加, 均以淹水 30 天为节点, 第一阶段变化更明显, 30 天后缓慢增长, 原土可氧化态锑变化最显著, 从 43.2mg/kg 增加至 89.4mg/kg, 增加了 107%。载铁土和载锰土中可氧化态锑含量从 112mg/kg 和 37.2mg/kg 增至 160mg/kg 和 57.9mg/kg, 分别增加了 43.3% 和 55.8%。可氧化态锑含量顺序为: 载铁土>原土>载锰土, 与原土相比, 载铁土可氧化态锑含量高于原土的 74.3% ~ 159%, 载锰土中可氧化态锑含量低于原土约 16.2% ~ 58.5%。可氧化态锑是与有机质活性基团结合的锑形态以及硫化物中被氧化为可溶性硫酸盐形式的锑形态。负载的 α-FeOOH 对锑的吸附作用强, 不仅可以吸附锑, 也能与有机质 (HA) 结合, 通过生成三元配合物 Fe-Sb-HA、Fe-HA-Sb 等形式固定锑。负载的 δ-MnO_2 也能吸附锑, 但 δ-MnO_2 上的 Mn(Ⅳ) 具有较强的氧化作用, 与有机质发生氧化还原反应, 使有机质活性基团结合的锑释放出来, 可能向弱酸提取态和可还原态转化。

由图 5d 可知, 原土残渣态锑含量随淹水时间延长逐渐增加, 从 15819mg/kg 增加至 17286mg/kg, 增加了 9.30%。载铁土和载锰土残渣态锑在淹水 30 ~ 60 天出现较大变化, 但随着淹水时间的延长到 180 天, 总体变化非常小, 分别为 1.60% 和 0.830%。本次实验土壤锑主要以残渣态形式存在, 占比在 97.5% 以上, 残渣态锑是存在于硅酸盐晶格中的锑形态, 最稳定, 不容易被破坏。

总之, 原土、载铁土和载锰土各形态锑含量变化趋势大部分在淹水 30 天发生转变, 与各形态铁和锰

含量的变化趋势转变点一致，说明土壤各形态铁和锰的变化可能促进了各形态锑的转化，特别是载铁土，载量大，负载的铁以活性大的无定形为主，其对锑形态转化的影响不容忽视。

2.4　淹水时间与土壤各形态锑和各形态铁锰相关性分析结果

淹水时间、悬浮液锑、土壤各形态锑、土壤各形态铁、土壤各形态锰之间的相关性分析结果如图 6 所示。从图 6 可知，在原土中，淹水时间与悬浮液锑、弱酸提取态锑和可还原态锑呈显著负相关；与可氧化态锑和残渣态锑呈显著正相关；与无定形铁、络合铁呈显著正相关；与游离锰、无定形锰和络合锰呈显著正相关。悬浮液锑和弱酸提取态锑均与游离锰、无定形铁/锰、络合铁呈显著负相关；可还原态锑与无定形铁、络合铁、游离锰、无定形锰均为显著负相关；可氧化态锑和残渣态锑均与游离锰、无定形铁/锰、络合铁/锰呈显著正相关。

从图 7 可知，载铁土中，淹水时间与悬浮液锑、可还原态锑显著负相关，与弱酸提取态锑和可氧化态锑呈显著正相关；分别与络合铁、游离铁呈显著正相关、负相关。悬浮液锑与游离铁呈显著正相关，与络合铁呈显著负相关；弱酸提取态锑和可还原态锑与络合铁分别呈显著正相关和负相关；可氧化态锑与游离铁呈显著负相关，与络合铁呈显著正相关。与原土相比，负载 α-FeOOH 后，淹水时间与弱酸提取态锑从负相关变成了正相关，随着淹水时间的延长，弱酸提取态锑整体呈上升的趋势，这是由于长时间淹水使无定形铁重结晶引起的，重结晶过程中吸附的锑被重新释放。

从图 8 可知，载锰土中，淹水时间与可氧化态锑呈显著正相关；与悬浮液锑和弱酸提取态锑呈显著负相关；与络合锰及游离锰的负相关性较强。与原土相比，负载 δ-MnO_2 后，淹水时间与可还原态锑从显著负相关转化为没有显著相关性。弱酸提取态锑与络合锰显著正相关；可还原态锑与游离锰和无定形锰显著相关；残渣态锑与游离锰、无定形锰和络合锰均呈显著正相关。载锰后，各形态锑与多种形态锰的相关性减弱。

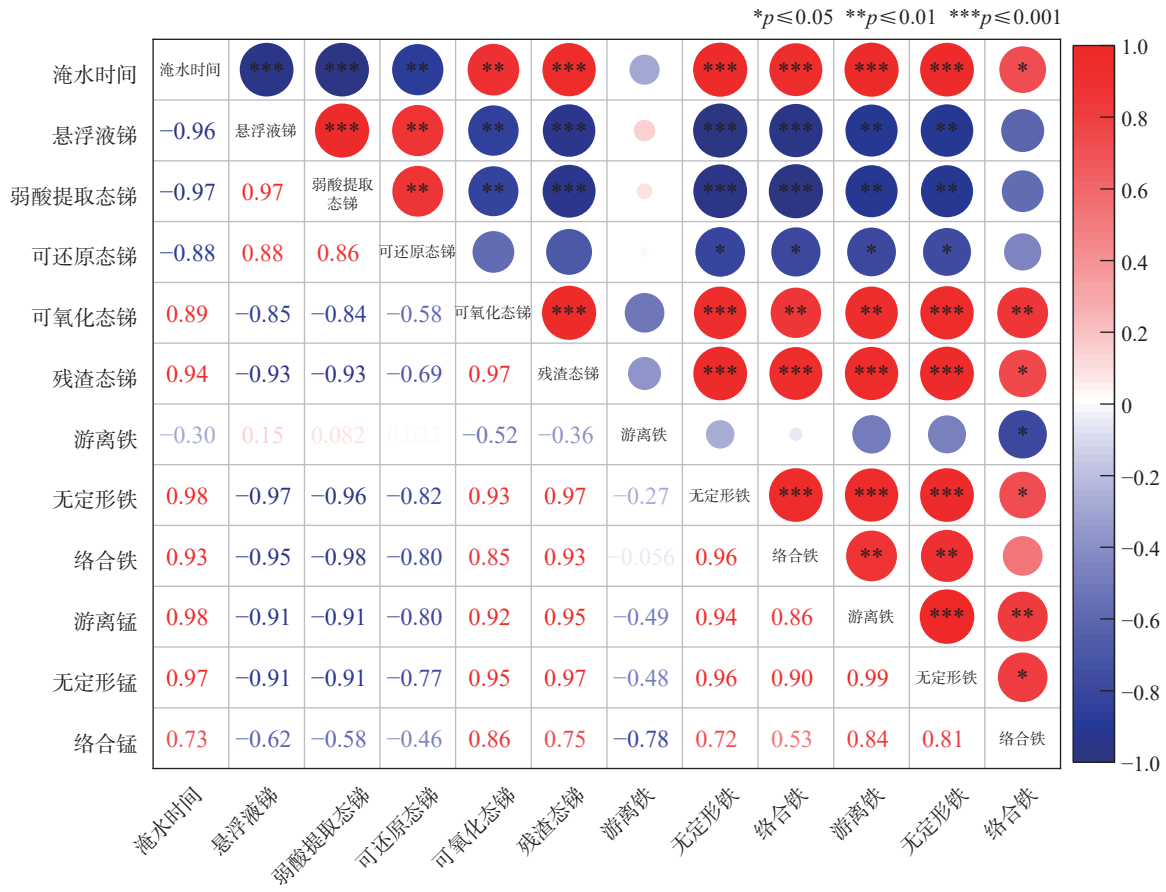

图6　淹水时间与土壤各形态锑、各形态铁、各形态锰之间的相关性分析结果 (原土)

Fig. 6　Correlation analysis results between flooding time and various forms of antimony, iron and manganese in original soil.

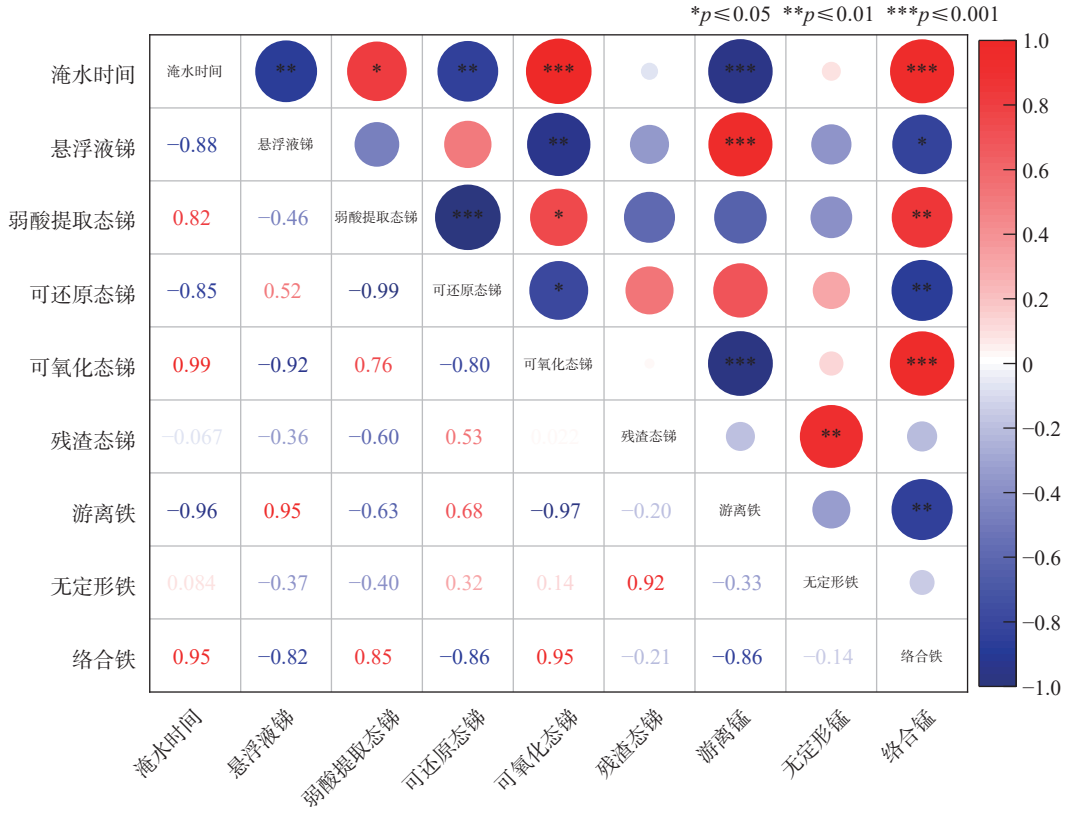

图7　淹水时间与土壤各形态锑、各形态铁之间的相关性分析结果 (载铁土)

Fig. 7　Correlation analysis results between flooding time and various forms of antimony and iron in Fe-loaded soil.

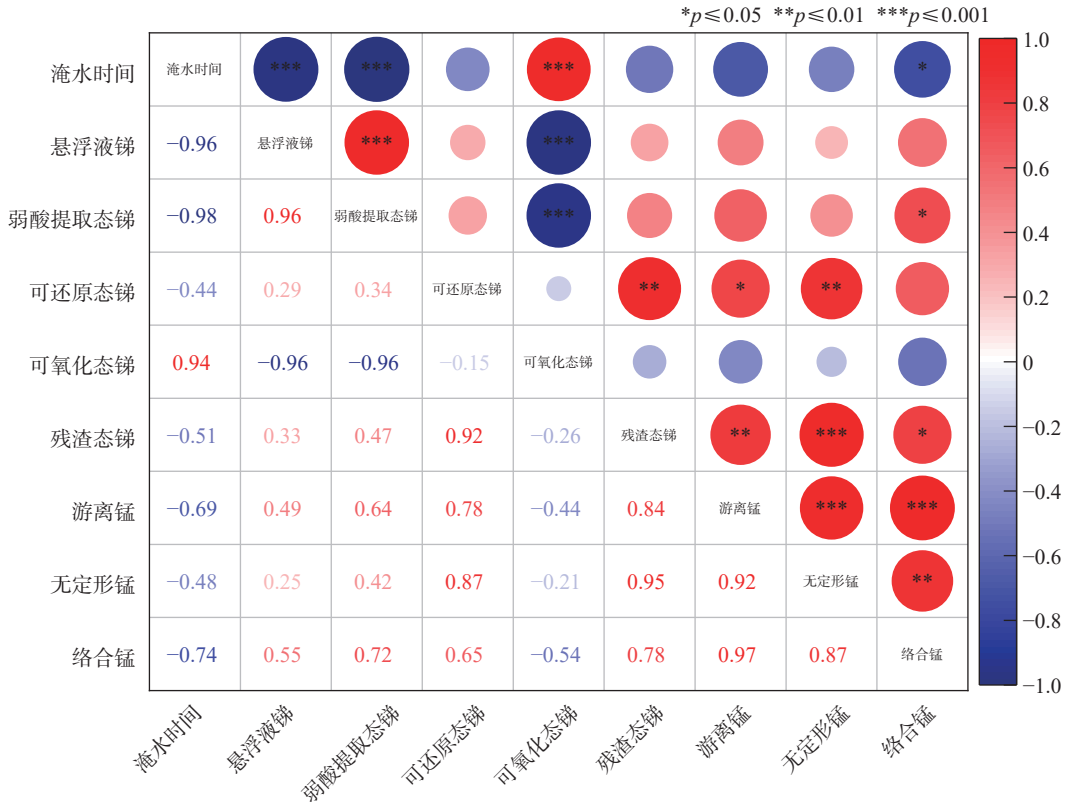

图8　淹水时间与土壤各形态锑、各形态锰之间的相关性分析结果 (载锰土)

Fig. 8　Correlation analysis results between flooding time and various forms of antimony and manganese in Mn-loaded soil.

原土中,各形态锑与多种形态的铁和锰具有显著相关性,淹水通过改变土壤氧化还原特性影响土壤中铁锰氧化物的赋存形态,进一步影响锑的形态分布。针铁矿通过其表面丰富的羟基官能团,能够强烈吸附锑,尤其是将可溶性的 Sb(Ⅲ) 和 Sb(Ⅴ) 转化为稳定的表面络合物。水钠锰矿则具有较强的氧化能力,能够将毒性较高的 Sb(Ⅲ) 氧化为毒性较低的 Sb(Ⅴ),同时通过吸附和共沉淀作用固定锑,进一步抑制其在土壤中的活性。所以,载铁和载锰后,打破了土壤中铁锰氧化物的形态平衡状态,因而影响到锑的形态转化,特别是载铁,负载的铁量大,且主要以无定形形式存在,对锑形态的影响更显著。

3　结论

通过原土、载铁土和载锰土淹水 180 天,探究了 α-FeOOH 和 δ-MnO_2 对土壤锑形态转化的影响。负载 α-FeOOH 降低了悬浮液中锑、土壤弱酸提取态锑,增加了土壤可还原态锑和可氧化态锑含量。负载 δ-MnO_2 增加了悬浮液中锑、土壤弱酸提取态锑、可还原态锑含量,降低了土壤可氧化态锑含量。原土/载铁土/载锰土各形态铁、锰、锑在淹水 30 天变化明显或变化趋势发生转折,淹水改变了土壤氧化还原特性,因而影响铁锰氧化物的赋存形态,进一步影响锑的形态分布。

本文以原位生成方式在矿区锑污染黄壤上负载 α-FeOOH 和 δ-MnO_2,并经过长达 180 天的反应,研究方式区别于现有研究,最大限度地模拟自然土壤生态环境,探究了铁锰氧化物及其形态的变化对土壤锑形态分布的影响机制。研究成果揭示了土壤中铁锰氧化物形态多样性对锑形态转化的关键调控作用,未来需在机制深度、多因子耦合及实际应用层面进一步突破,以推动铁锰基材料在矿区土壤锑污染修复中的科学化与工程化应用,更好地服务于绿色矿山建设。

Effects of Goethite/Birnessite on Antimony Speciation in Yellow Soil from an Antimony Mining Area under Simulated Natural Conditions

LIU Jingguang[1], *ZHAO Ping*[2*], *REN Wei*[2], *MA Xue*[1], *HE Kaiying*[1], *ZHU Xiaping*[1*]

(1. College of Materials and Chemistry & Chemical Engineering (College of Lithium Resources and Lithium Battery Industry), Chengdu University of Technology, Chengdu 610059, China;
2. No.105 Geological Brigade, Guizhou Bureau of Geology and Mineral Resources Exploration and Development, Guiyang 550018, China)

HIGHLIGHTS

(1) α-FeOOH and δ-MnO_2 are the most active components of clay minerals in soil, affecting the transformation of antimony speciation in soil. Fe-loaded soil and Mn-loaded soil were obtained through *in situ* loading 4.0% α-FeOOH (calculated as Fe) and 0.1% δ-MnO_2 (calculated as Mn).

(2) The loaded α-FeOOH was predominantly amorphous iron in the soil, and the loaded δ-MnO_2 existed in various forms of manganese in soil.

(3) After 30 days of flooding, the speciation of iron, manganese, and antimony in the original, Fe-loaded, and Mn-loaded soils exhibited significant changes or turning points. Flooding altered iron and manganese oxide forms in the soils, thereby promoting antimony speciation transformation.

ABSTRACT: The antimony (Sb) mining area and its surrounding soil are severely polluted with antimony, and the degree of antimony pollution is closely related to its speciation in the soil. Iron and manganese oxides are the most active components of clay minerals in soil, affecting the transformation of antimony speciation in soil. Existing research focuses more on the effect of single iron and manganese oxides on the adsorption of exogenous antimony, while basic study on the effect of iron and manganese oxides on the transformation of antimony speciation in actual soil needs to be strengthened. This study described the *in situ* preparation of goethite (α-FeOOH) and birnessite (δ-MnO_2) in soil, which were loaded onto antimony contaminated yellow soil (original soil) in the Qinglong antimony mining area, Guizhou Province to obtain Fe-loaded soil and Mn-loaded soil. Simulating the natural soil conditions, a 180-day flooding experiment of original soil, Fe-loaded soil and Mn-loaded soil was conducted. The transformation characteristics of soil antimony forms mediated by α-FeOOH and δ-MnO_2 were explored. The results showed that flooding changed the redox characteristics of soil, affected the forms of iron and manganese oxides, and thus affected the distribution of antimony speciation. The loaded α-FeOOH mainly existed as amorphous iron, while the loaded δ-MnO_2 existed in three forms: free manganese, amorphous manganese, and complex manganese. Compared with the original soil, the content of Sb in the suspension and weak acidic extracted antimony of Fe-loaded soil decreased by 88.3%−94.4% and 21.1%−65.9%, respectively; the content of reducible antimony and oxidizable antimony increased by 49.0%−67.2% and 74.3%−159%, respectively; Sb in the suspension, weak acidic extracted antimony, and reducible antimony in Mn-loaded soil increased by 14.2%−59.5%, 6.50%−32.6%, and 4.80%−23.3%, respectively, while oxidizable antimony decreased by 16.2%−58.5%. The various speciation of iron, manganese, and antimony in the original soil, Fe-loaded soil and Mn-loaded soil showed significant changes or a turning point in the trend after 30 days of flooding. Loading α-FeOOH promoted the transformation of weak acidic extracted antimony to reducible and oxidizable antimony in the soil, while loading δ-MnO_2 promoted the transformation of oxidizable antimony to weak acidic extracted antimony and reducible antimony in the soil. This study provides a key scientific basis for the risk assessment and remediation technology of antimony contaminated soil. In the future, the control of soil antimony pollution needs to be combined with the regulation of iron and manganese oxide forms and the management of redox conditions to achieve long-term stabilization of antimony. The BRIEF REPORT is available for this paper at http://www.ykcs.ac.cn/en/article/doi/10.15898/j.ykcs.202502280032.

KEY WORDS: α-FeOOH; δ-MnO_2; soil; antimony; speciation transformation; atomic absorption spectroscopy

BRIEF REPORT

Significance: Antimony (Sb) is a heavy metal with high toxicity and carcinogenicity. The issue of soil antimony contamination in global antimony mining areas and their surrounding regions is particularly severe. In the Qinglong antimony mining area of Guizhou, China, soil antimony concentration reaches up to 23559mg/kg, far exceeding the WHO-recommended safety limit (36mg/kg), posing significant threats to local ecosystems and human health [6-7].

The toxicity of antimony is closely linked to its speciation in soil [8]. Different antimony speciation in soil exists in dynamic equilibrium. The more reactive Fe/Mn oxides are the main factors influencing the distribution and transformation of soil antimony speciation [9-10]. Goethite (α-FeOOH), the most common iron oxide in soil, exhibits a large specific surface area and abundant hydroxyl groups on its surface, providing numerous active sites with strong chemical affinity for antimony [19-20]. Goethite demonstrates excellent adsorption capacity for Sb(Ⅲ) across a broad pH range (3–12), while maximum adsorption of Sb(Ⅴ) occurs at pH<7 [21]. Birnessite (δ-MnO_2), the optimal reactive mineral phase for antimony retention in soil, not only adsorbs both Sb(Ⅲ) and Sb(Ⅴ) but also oxidizes Sb(Ⅲ) via surface Mn(Ⅳ) [25-26].

However, existing studies primarily focus on short-term adsorption performance and mechanisms of single

Fe/Mn oxides for antimony, lacking systematic exploration of the long-term dynamic transformations of Fe/Mn oxides and their forms in complex soil systems and their regulatory effects on antimony speciation. Therefore, for this study, *in situ* α-FeOOH and δ-MnO_2 was loaded onto Sb-contaminated yellow soil from the Qinglong antimony mining area in Guizhou Province, preparing Fe-loaded soil and Mn-loaded soil. A 180-day flooding experiment was conducted to systematically analyze antimony speciation in soils under prolonged alternating redox conditions, investigating the impacts of Fe/Mn oxides and their forms on antimony speciation transformation.

Methods: The tested soil was collected from the Qinglong antimony mining area in Guizhou Province. The soil pH is 4.20, and the antimony content is 16796mg/kg, belonging to strong acid and high pollution yellow soil. Fe-loaded soil and Mn-loaded soil were prepared by loading 4.0% α-FeOOH (calculated as Fe) and 0.1% δ-MnO_2 (calculated as Mn) by *in situ* chemical precipitation method.

Weigh 20.0g antimony contaminated yellow soil (original soil), Fe-loaded soil and Mn-loaded soil respectively in a 100mL beaker, add 30mL ultrapure water at the water-soil ratio of 1∶1.5, and flood for 10, 20, 30, 60, 90, 120, 150 and 180 days, and set three parallel treatments at each time. During flooding, the volatile water shall be supplemented by weighing method every few days and stirred evenly. After the experiment, centrifuge and determine the concentrations of antimony, iron, and manganese in the suspension. Dry the soil and pass it through a 60-mesh sieve, then determine the concentrations of antimony, iron, and manganese in the soil in different forms.

Free iron/manganese was extracted using the sodium hydrosulfite sodium citrate method; Amorphous iron/manganese was prepared using ammonium oxalate buffer solution (pH=3.2); Complex iron/manganese was extracted using sodium pyrophosphate solution (pH=8.5). Antimony speciation was extracted according to GB/T 25282—2010 classification. The various speciation of iron, manganese, and antimony were determined using AA-7001 atomic absorption spectroscopy. The instrument parameters for measuring antimony/iron/manganese were: wavelength of 217.6nm/248.3nm/279.5nm, lamp current of 4mA/3mA/3mA, and slit width of 0.2nm.

Data and Results: The loaded α-FeOOH mainly existed in amorphous iron, while the loaded δ-MnO_2 existed in free manganese, amorphous manganese and complex manganese.

The content of weak acid extracted antimony in original soil and Mn-loaded soil decreased with the extension of flooding time, from 123mg/kg and 140mg/kg to 71.9mg/kg and 107mg/kg, respectively, decreasing by 41.5% and 23.6%, respectively. The content of weak acid extracted antimony in Fe-loaded soil decreased first and then increased with the extension of flooding time, and the content of weak acid extracted antimony increased by 31.3% overall. Compared with the original soil, the content of weak acid extracted antimony in Fe-loaded soil decreased by 21.1%−65.9%. On the contrary, the content of weak acid extracted antimony in Mn-loaded soil was 6.50%−32.6% higher than that in the original soil.

The content of reducible antimony in original soil, Fe-loaded soil and Mn-loaded soil increased at first and then decreased with the extension of flooding time. The content of reducible antimony in the original soil increased by 16.6% in the first stage (0−30d) and decreased by 28.1% in the second stage (30−180d); overall, the reducible antimony content decreased by 16.2%. The content of reducible antimony in the first stage (0−30d) and second stage (30−180d) of Fe-loaded soil increased by 15.7% and decreased by 21.9%, respectively. The content of reducible antimony in Mn-loaded soil increased by 14.7% in the first stage (0−30d) and decreased by 16.8% in the second stages (30−180d), respectively, and the overall change was only 1.80%. The order of reducible antimony content was Fe-loaded soil>Mn-loaded soil>the original soil. The content of reducible antimony in Fe-loaded soil and Mn-loaded soil was higher than that in the original soil by 49.0%−67.2% and 4.80%−23.3%, respectively.

The content of oxidable antimony in the original soil, Fe-loaded soil and Mn-loaded soil increased gradually with the extension of flooding time, with more obvious changes in the first stage (0−30d) and slower growth in the second stage (30−180d). The change of oxidable antimony in the original soil was the most significant, from

43.2mg/kg to 89.4mg/kg, an increase of 107%. The content of oxidized antimony in Fe-loaded soil and Mn-loaded soil increased from 112mg/kg and 37.2mg/kg to 160mg/kg and 57.9mg/kg, increased by 43.3% and 55.8%, respectively. Compared with the original soil, the content of oxidable antimony in Fe-loaded soil was higher than that in the original soil by 74.3%−159%, and the content of oxidable antimony in the Mn-loaded soil was lower than that in the original soil by 16.2%−58.5%.

The content of residual antimony in the original soil increased from 15819mg/kg to 17286mg/kg, an increase of 9.30%. Residual antimony in Fe-loaded soil and Mn-loaded soil changed greatly from 30 to 60 days after flooding, but with the extension of flooding time to 180 days, the overall change was very small, 1.60% and 0.830%, respectively.

In summary, the speciation of iron, manganese and antimony in original soil, Fe-loaded soil and Mn-loaded soil changed significantly or had a reversal of trend after 30 days of flooding. Loading α-FeOOH promoted the transformation of weak acid extracted antimony to reducible antimony and oxidizable antimony, and loading δ-MnO_2 promoted the transformation of oxidizable antimony to weak acid extracted antimony and reducible antimony.

参考文献

[1] 米艳华, 雷梅, 黎其万, 等. 滇南矿区重金属污染耕地的植物修复及其健康风险[J]. 生态环境学报, 2016, 25(5): 864−871.
Mi Y H, Lei M, Li Q W, et al. Plant remediation and health risks of heavy metal contaminated farmland in southern Yunnan mining area[J]. Journal of Ecological Environment, 2016, 25(5): 864−871.

[2] Mbadugha L, Cowper D, Dossanov S, et al. Geogenic and anthropogenic interactions at a former Sb mine: Environmental impacts of As and Sb[J]. Environmental Geochemistry and Health, 2020, 42: 11−24.

[3] Ning Z P, Xiao T F, Xiao E Z. Antimony in the soil-plant system in an Sb mining/smelting area of Southwest China[J]. International Journal of Phytoremediation, 2015, 17(11): 1081−1089.

[4] 李聪, 杨爱江, 陈蔚洁, 等. 锑胁迫对鱼腥草抗氧化能力及渗透调节物质的影响[J]. 江苏农业科学, 2019, 47(13): 175−179.
Li C, Yang A J, Chen W J, et al. The effect of antimony stress on the antioxidant capacity and osmoregulatory substances of Houttuynia cordata[J]. Jiangsu Agricultural Sciences, 2019, 47(13): 175−179.

[5] 莫昌琍, 吴丰昌, 符志友, 等. 湖南锡矿山锑矿区农用土壤锑、砷及汞的污染状况初探[J]. 矿物学报, 2013, 33(3): 344−350.
Mo C L, Wu F C, Fu Z Y, et al. Preliminary study on the pollution status of antimony, arsenic, and mercury in agricultural soil of tin mine antimony mining area in Hunan Province[J]. Acta Mineralogica Sinica, 2013, 33(3): 344−350.

[6] Ren W, Ran Y Y, Mou Y W, et al. Pollution characteristics and risk assessment of antimony and arsenic in a typical abandoned antimony smelters[J]. Environmental Geochemistry and Health, 2023, 45(7): 5467−5480.

[7] Lai Z Y, He M C, Lin C Y, et al. Interactions of antimony with biomolecules and its effects on human health[J]. Ecotoxicology and Environmental Safety, 2022, 233: 113317.

[8] 谢晓峰. 贵州晴隆锑矿山废弃物中锑的表生迁移转化过程和机制[D]. 贵阳: 贵州大学, 2023.
Xie X F. Surface migration and transformation process and mechanism of antimony in Qinglong antimony mine waste in Guizhou Province[D]. Guiyang: Guizhou University, 2023.

[9] 李婉霞, 陈梅青, 刘奕安, 等. 水钠锰矿界面铁矿物的形成对 Sb 迁移转化的影响机理[J]. 中国环境科学, 2025, 45(3): 1341−1350.
Li W X, Chen M Q, Liu Y A, et al. Mechanism of the influence of iron mineral formation at the interface of sodium manganese ore on antimony migration and transformation[J]. China Environmental Science, 2025, 45(3): 1341−1350.

[10] 崔婷, 叶欣, 朱霞萍, 等. 土壤铁锰氧化物形态测定及吸附 Sb(Ⅲ) 的主控因子研究[J]. 岩矿测试, 2023, 42(1): 167−176.
Cui T, Ye X, Zhu X P, et al. Determination of soil iron

and manganese oxide forms and study on the main control factors of Sb(Ⅲ) adsorption[J]. Rock and Mineral Analysis, 2023, 42(1): 167−176.

[11] 胡敏, 李芳柏. 土壤微生物铁循环及其环境意义[J]. 土壤学报, 2014, 51(4): 683−698.
Hu M, Li F B. Soil microbial iron cycling and its environmental significance[J]. Journal of Soil Science, 2014, 51(4): 683−698.

[12] Cornell R M, Schwertmann U. The iron oxides: Structure, properties, reactions, occurrences, and uses[M]. Clay Minerals, 1999, 34(1): 209−211.

[13] 郭贵宾, 袁晓雅, 黄理金, 等. 土壤中典型矿物对锑的吸附-沉积行为研究[J]. 岩矿测试, 2025, 44(1): 127−139.
Guo G B, Yuan X Y, Huang L J, et al. Study on the adsorption deposition behavior of typical minerals in soil towards antimony[J]. Rock and Mineral Analysis, 2025, 44(1): 127−139.

[14] Zhou W Q, Zhou J W, Feng X B, et al. Antimony isotope fractionation revealed from EXAFS during adsorption on Fe(oxyhydr)oxides[J]. Environmental Science & Technology, 2023, 57(25): 9353−9361.

[15] Yu S H, Wang Y, Wan Y Y, et al. Enhance antimony adsorption from aquatic environment by microwave-assisted prepared Fe_3O_4 nanospherolites[J]. Environmental Science and Pollution Research, 2023, 30(41): 94401−94413.

[16] 向超, 王媛媛, 曾嘉庆, 等. 冶炼渣堆周边土壤砷锑垂向迁移分布及影响因素[J]. 中国有色金属学报, 2024, 34(8): 2773−2786.
Xiang C, Wang Y Y, Zeng J Q, et al. Vertical migration distribution and influencing factors of arsenic and antimony in the soil around the smelting slag heap[J]. The Chinese Journal of Nonferrous Metals, 2024, 34(8): 2773−2786.

[17] Xu W, Wang H J, Liu R P, et al. The mechanism of antimony(Ⅲ) removal and its reactions on the surfaces of Fe-Mn binary oxide[J]. Journal of Colloid and Interface Science, 2011, 363(1): 320−326.

[18] Mitsunobu S, Muramatisu C, Watanabe K, et al. Behavior of antimony(Ⅴ) during the transformation of ferrihydrite and its environmental implications[J]. Environmental Science & Technology, 2013, 47(17): 9660−9667.

[19] Kuang L Y, Liu Y Y, Fu D D, et al. FeOOH-graphene oxide nanocomposites for fluoride removal from water: Acetate mediated nano FeOOH growth and adsorption mechanism[J]. Journal of Colloid and Interface Science, 2017, 490: 259−269.

[20] Liu Z G, Zhang F S. Removal of lead from water using biochars prepared from hydrothermal liquefaction of biomass[J]. Journal of Hazardous Materials, 2009, 167(1-3): 933−939.

[21] Zhou C C, Li C, Yang K L, et al. Sb(Ⅴ) removal by different iron oxides from simulated textile-wastewater[J]. Acta Scientiae Circumstantiae, 2022, 42(2): 96−107.

[22] Burton E D, Hockmann K, Karimian N. Antimony sorption to goethite: Effects of Fe(Ⅱ)-catalyzed recrystallization[J]. ACS Earth and Space Chemistry, 2020, 4(3): 476−487.

[23] Shangguan Y X, Qin X P, Zhao L, et al. Effects of iron oxide on antimony(V) adsorption in natural soils: Transmission electron microscopy and X-ray photoelectron spectroscopy measurements[J]. Journal of Soils & Sediments, 2016, 16(2): 509−517.

[24] Guo W J, Fu Z Y, Wang H, et al. Removal of antimonate (Sb(Ⅴ)) and antimonite (Sb(Ⅲ)) from aqueous solutions by coagulation-flocculation-sedimentation (CFS): Dependence on influencing factors and insights into removal mechanisms[J]. Science of the Total Environment, 2018, 644: 1277−1285.

[25] Lu H B, Han X G, Ren J M, et al. Enhanced removal of Sb(Ⅲ) and Sb(Ⅴ) by acid birnessite with doped titanium ions[J]. Technology of Water Treatment, 2023, 49(8): 30−39.

[26] Sun Q, Liu C, Alves M E, et al. The oxidation and sorption mechanism of Sb on δ-MnO_2[J]. Chemical Engineering Journal, 2018, 342: 429−437.

[27] Sun W N, Sun X X, Li B Q, et al. Bacterial response to antimony and arsenic contamination in rice paddies during different flooding conditions[J]. Science of the Total Environment, 2019, 675: 273−285.

[28] 崔晓丹, 王玉军, 周东美. 水分管理对污染土壤中砷锑形态及有效性的影响[J]. 农业环境科学学报, 2015, 34(9): 1665−1673.
Cui X D, Wang Y J, Zhou D M. The impact of water management on the forms and availability of arsenic and

antimony in polluted soil[J]. Journal of Agro-Environmental Science, 2015, 34(9): 1665−1673.

[29] 张又弛, 唐晓达, 罗文邃. 淹水还原条件下红壤中葡萄糖及腐植酸对铁锰形态的影响[J]. 土壤学报, 2014, 51(2): 270−277.
Zhang Y C, Tang X D, Luo W S. The effect of glucose and humic acid on iron and manganese forms in red soil under flooding reduction conditions[J]. Journal of Soil Science, 2014, 51(2): 270−277.

[30] 姚冬菊, 刘恩光, 宁增平, 等. 贵州某锑冶炼厂周边农田土壤锑、砷污染与人体健康风险评估[J]. 地球与环境, 2021, 49(6): 673−683.
Yao D J, Liu E G, Ning Z P, et al. Assessment of soil antimony and arsenic pollution and human health risks in the surrounding farmland of an antimony smelter in Guizhou Province[J]. Earth and Environment, 2021, 49(6): 673−683.

[31] 吴琼, 张洋, 孟昭福. 十二烷基二甲基甜菜碱 (BS-12) 在合成针铁矿表面的吸附特征[J]. 环境科学学报, 2019, 39(9): 3045−3052.
Wu Q, Zhang Y, Meng Z F. Adsorption characteristics of dodecyl dimethyl betaine (BS-12) on the surface of synthetic goethite[J]. Journal of Environmental Science, 2019, 39(9): 3045−3052.

[32] 梁慧锋, 马子川, 刘占牛. 新生态二氧化锰的性质及pH 值影响除砷效果的研究[J]. 无机化学学报, 2006, 22(4): 743−747.
Liang H F, Ma Z C, Liu Z N. Study on the properties of new ecological manganese dioxide and the influence of pH value on arsenic removal efficiency[J]. Journal of Inorganic Chemistry, 2006, 22(4): 743−747.

[33] 冉继伟, 张旭, 宁平, 等. 全国主要土壤铁重金属形态及其与土壤性质的关系[J]. 环境科学导刊, 2017, 36(4): 1−4.
Ran J W, Zhang X, Ning P, et al. The forms of iron and heavy metals in major soils nationwide and their relationship with soil properties[J]. Environmental Science Survey, 2017, 36(4): 1−4.

[34] 何群, 陈家坊. 土壤中游离铁和络合态铁的测定[J]. 土壤, 1983, 1(6): 242−244.
He Q, Chen J F. Determination of free iron and complexed iron in soil[J]. Soil, 1983, 1(6): 242−244.

[35] 徐晨瀛, 胡启武, 张桂华, 等. 鄱阳湖湿地剖面土壤铁结合态有机碳沿高程的分布特征[J]. 应用生态学报, 2024, 35(12): 3488−3496.
Xu C Y, Hu Q W, Zhang G H, et al. Distribution characteristics of soil iron bound organic carbon along elevation in Poyang Lake wetland profile[J]. Journal of Applied Ecology, 2024, 35(12): 3488−3496.

[36] Villalobos M, Toner B, Bargar J, et al. Characterization of the manganese oxide produced by pseudomonas putida strain MnB1[J]. Geochimica et Cosmochimica Acta, 2003, 67(14): 2649−2662.